Zero-index structures as an alternative platform for quantum optics

Iñigo Liberal[a] and Nader Engheta[a,1]

[a]Department of Electrical and Systems Engineering, University of Pennsylvania, Philadelphia, PA 19104

Edited by Marlan O. Scully, Texas A&M, College Station, TX, and approved December 16, 2016 (received for review July 20, 2016)

Vacuum fluctuations are one of the most distinctive aspects of quantum optics, being the trigger of multiple nonclassical phenomena. Thus, platforms like resonant cavities and photonic crystals that enable the inhibition and manipulation of vacuum fluctuations have been key to our ability to control light–matter interactions (e.g., the decay of quantum emitters). Here, we theoretically demonstrate that vacuum fluctuations may be naturally inhibited within bodies immersed in epsilon-and-mu-near-zero (EMNZ) media, while they can also be selectively excited via bound eigenmodes. Therefore, zero-index structures are proposed as an alternative platform to manipulate the decay of quantum emitters, possibly leading to the exploration of qualitatively different dynamics. For example, a direct modulation of the vacuum Rabi frequency is obtained by deforming the EMNZ region without detuning a bound eigenmode. Ideas for the possible implementation of these concepts using synthetic implementations based on structural dispersion are also proposed.

metamaterial | quantum optics | near-zero refractive index | ENZ | vacuum fluctuation

Vacuum fluctuations, the fluctuations of a quantized field on its vacuum state around its zero average (1), are considered one of the most distinctive (1–3) and disputed (4) aspects of quantum optics and quantum field theory. Although direct measurements of vacuum fluctuations have only been proposed very recently (5), they are the attributed source of numerous nonclassical phenomena, including, for instance, spontaneous emission (6), Lamb shift (7), Casimir forces (8), molecular energy transfer (9), quantum friction (10), as well as several vacuum amplification effects (3). It is also a well-established fact that macroscopic bodies modify the structure of electromagnetic fields, opening up the possibility of engineering all aforementioned effects (6, 11). For example, because quantum fields fluctuate in a space empty of matter, we could ask what should be the matter filling the space to first inhibit and then selectively engineer vacuum fluctuations (Fig. 1*A*). Traditional answers to this question have appeared in the form of photonics crystals (PCs) (12–15) and closed cavities (16–18), leading to formidable advances in the ability to control light–matter interactions. In essence, the geometry of periodic structures and resonators can be engineered in such a way so that they do not support eigenmodes on a given frequency range. Here, we demonstrate theoretically that epsilon-mu-near-zero (EMNZ) media (19), also known as matched zero-index (ZI) media (20), that is, a medium with simultaneously zero permittivity and permeability, behaves as a natural inhibitor of vacuum fluctuations. Thus, we propose ZI structures as an alternative platform to manipulate spontaneous emission, and other related effects, possibly leading to the exploration of qualitatively different decay dynamics.

Note than one could conceivably approach this problem by using a canonical quantization procedure (1). In this manner, we could consider a space filled with a substance of refractive index n, and carry out the conventional quantization approach based on a cubic cavity of side L (1). In doing so, it is evident that the density of states obtained in the $L\to\infty$ limit, $\rho(\omega)=n^3(\omega^2/\pi^2c^3)$, would be completely depleted in media with a zero-refractive index $n\to 0$. This analysis presents an interesting perspective, in which ZI media can be considered somewhat analogous to PCs materials and closed cavities in as far as they deplete the space of electromagnetic modes. However, despite providing a nice intuition, this model does not capture the necessary dispersive properties of ZI media (19). Moreover, it also fails to account for the interaction of a small quantum system [e.g., a quantum emitter (QE) such as an atom or a quantum dot] and macroscopic media, because the QE must be insulated from the background macroscopic bodies to produce a consistent result (21, 22). However, this preliminary consideration identifies ZI media as a potential candidate to inhibit vacuum fluctuations and spontaneous emission.

Macroscopic Quantum Electrodynamics

Therefore, to elucidate the main features of vacuum fluctuations in the presence of ZI media, as well as their interaction with QEs, we describe the system by using the known macroscopic quantum electrodynamics tools developed for the analysis of dispersive media (6, 23). For the sake of simplicity, we assume that the space is filled with an inhomogeneous medium characterized by relative permittivity, $\varepsilon(\mathbf{r},\omega)=\varepsilon_{\mathrm{R}}(\mathbf{r},\omega)+\mathrm{i}\,\varepsilon_{\mathrm{I}}(\mathbf{r},\omega)$, and relative permeability, $\mu(\mathbf{r},\omega)=\mu_{\mathrm{R}}(\mathbf{r},\omega)+\mathrm{i}\,\mu_{\mathrm{I}}(\mathbf{r},\omega)$. Under this framework, the excitations of the EM fields–matter system are represented by a continuum of harmonic oscillators with associated polaritonic operators $\hat{\mathbf{f}}_{\mathrm{q}}(\mathbf{r},\omega)$ $(\mathrm{q}=\mathrm{e},\mathrm{m})$. The Hamiltonian of this matter–field system is $\hat{\mathrm{H}}=\sum_{\mathrm{q=e,m}}\int \mathrm{d}\omega\int \mathrm{d}^3\mathrm{r}\;\hbar\omega\,\hat{\mathbf{f}}^{\dagger}_{\mathrm{q}}(\mathbf{r},\omega)\cdot\hat{\mathbf{f}}_{\mathrm{q}}(\mathbf{r},\omega)$, and the electric field operator is given by $\hat{\mathbf{E}}(\mathbf{r},\mathrm{t})=\int d\omega e^{-i\omega t}\,\hat{\mathbf{E}}(\mathbf{r},\omega)+\mathrm{h.c.}$, where $\hat{\mathbf{E}}(\mathbf{r},\omega)=\sum_{\mathrm{q=e,m}}\int d^3r'\;\mathbf{G}_{\mathrm{q}}(\mathbf{r},\mathbf{r}',\omega)\cdot\hat{\mathbf{f}}_{\mathrm{q}}(\mathbf{r}',\omega)$. Here, we use the definitions $\mathbf{G}_{\mathrm{e}}(\mathbf{r},\mathbf{r}',\omega)=\mathrm{i}\frac{\omega^2}{c^2}\sqrt{(\hbar/\pi\varepsilon_0)\varepsilon_I(\mathbf{r}',\omega)}\;\mathbf{G}(\mathbf{r},\mathbf{r}',\omega)$ and $\mathbf{G}_{\mathrm{m}}(\mathbf{r},\mathbf{r}',\omega)=-\mathrm{i}(\omega/c)\sqrt{(\hbar/\pi\varepsilon_0)\left(\mu_I(\mathbf{r}',\omega)/|\mu_I(\mathbf{r}',\omega)|^2\right)}\;\mathbf{G}(\mathbf{r},\mathbf{r}',\omega)\times\overleftarrow{\nabla}$, where $\mathbf{G}(\mathbf{r},\mathbf{r}',\omega)$ is the classical Green dyadic function of the

Significance

Metamaterials provide additional venues for routing and shaping waves, as well as manipulating wave–matter interactions. In principle, similar concepts and techniques could be applied to engineer the properties of quantized fields. Here, we theoretically demonstrate that structures with a near-zero refractive index are capable of inhibiting and then selectively exciting electric field vacuum fluctuations. This effect might offer different pathways to manipulate quantized fields with metamaterials. We illustrate this point by investigating the decay dynamics of a quantum emitter embedded in a zero-index shell. For this particular example, we theoretically show how the distinctive features of zero-index media enable unique phenomena, such as a direct modulation of the vacuum Rabi frequency by deforming the zero-index shell.

Author contributions: I.L. and N.E. conceived the idea; I.L. carried out the analytical modeling and numerical simulations; N.E. supervised the project; I.L. and N.E. contributed to the design of the problems, interpretation and analysis of the presented results, discussion and understanding of findings, and writing of the manuscript.

The authors declare no conflict of interest.

This article is a PNAS Direct Submission.

[1]To whom correspondence should be addressed. Email: engheta@ee.upenn.edu.

This article contains supporting information online at www.pnas.org/lookup/suppl/doi:10.1073/pnas.1611924114/-/DCSupplemental.

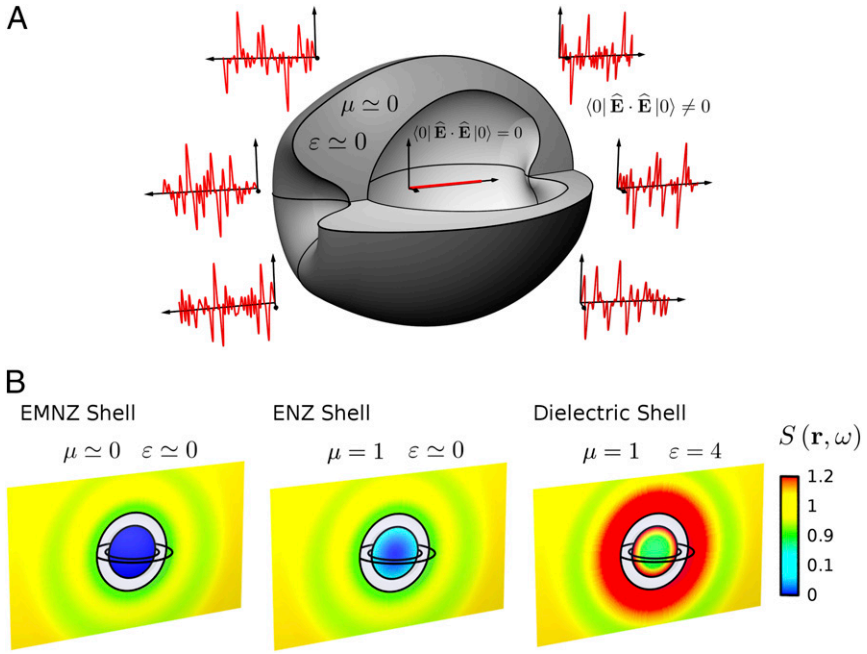

Fig. 1. Inhibiting and engineering vacuum fluctuations with macroscopic media. (*A*) Conceptual sketch of an epsilon-and-mu-near-zero (EMNZ), $\mu \approx \varepsilon \approx 0$, shell that inhibits vacuum (electric field) fluctuations within the region encapsulated by it. (*B*) Spectral density of vacuum (electric field) fluctuations, $S(\mathbf{r},\omega)$, normalized to its free-space counterpart, in the presence of ideally lossless EMNZ, epsilon-near-zero (ENZ) ($\mu = 1, \ \varepsilon \approx 0$) and dielectric ($\mu = 1, \ \varepsilon = 4$) spherical shells of internal and external radii $r_1 = 0.2\lambda$ and $r_2 = 0.3\lambda$, respectively.

background medium. See refs. 6 and 23 for more details of this quantization approach.

Vacuum Fluctuations

It can be readily checked from the above formalism that the expectation value of the electric field on its vacuum state is zero $\langle 0|\hat{\mathbf{E}}(\mathbf{r},t)|0\rangle = 0$. However, the expectation value of the field intensity operator is nonzero $\langle 0|\hat{\mathbf{E}}(\mathbf{r},t)\cdot\hat{\mathbf{E}}(\mathbf{r},t)|0\rangle \neq 0$, leading to the so-called vacuum fluctuations (1). Specifically, it can be demonstrated by using properties of the Green function $\mathbf{G}(\mathbf{r},\mathbf{r}',\omega)$ that vacuum fluctuations in the presence of macroscopic media can be compactly written as $\langle 0|\hat{\mathbf{E}}(\mathbf{r},t)\cdot\hat{\mathbf{E}}(\mathbf{r},t)|0\rangle = \int d\omega \, S(\mathbf{r},\omega)$, with $S(\mathbf{r},\omega) = (\hbar\mu_0/\pi)\omega^2 \, \mathrm{Tr}\{\mathrm{Im}\, \mathbf{G}(\mathbf{r},\mathbf{r},\omega)\}$ being defined as the spectral density of vacuum (electric field) fluctuations. For example, in free space, we have a uniform distribution $S(\mathbf{r},\omega) \to S_0(\mathbf{r},\omega) = (\hbar\mu_0/2\pi^2 c) \ \omega^3$.

However, $S(\mathbf{r},\omega)$ can be engineered by using macroscopic media, and next we find that $S(\mathbf{r},\omega) \to 0$ within bodies of arbitrary geometry immersed within an EMNZ body of arbitrary geometry. This effect can be demonstrated by noting that $\mathrm{Im}\, G_{uu}(\mathbf{r}',\mathbf{r}',\omega)$ is proportional to the time-averaged power supplied by a classical current moment $\mathbf{J}(\mathbf{r}) = \hat{\mathbf{u}} \, Idl\delta(\mathbf{r}-\mathbf{r}')$ located at $\mathbf{r}'$, oriented along $\hat{\boldsymbol{u}}$, and oscillating at frequency ω: $P_{sup} = -(1/2)\int_V \mathrm{Re}\{\mathbf{E}\cdot\mathbf{J}^*\}dV = (\omega\mu_0/2)\,|Idl|^2 \, \mathrm{Im}\, G_{uu}(\mathbf{r}',\mathbf{r}',\omega)$ (24). In addition, it follows from Poynting's theorem that, for vanishingly small losses, P_{sup} equals the power radiated outside the EMNZ body by this classical source (24). Furthermore, we note that EMNZ forms the so-called a DB boundary (25), that is, because $\mathbf{D} = 0$ and $\mathbf{B} = 0$ within the EMNZ body, then the normal components of the $\mathbf{E}$ and $\mathbf{H}$ must vanish in the external surface of the EMNZ body to satisfy the continuity of $\hat{\mathbf{n}}\cdot\mathbf{D}$ and $\hat{\mathbf{n}}\cdot\mathbf{B}$ across the interface. However, it can be proven (26) that fields outside the EMNZ body are uniquely determined by the normal components of the $\mathbf{E}$ and $\mathbf{H}$. Therefore, this is sufficient to prove that, if a classical dipole is located within a body immersed in a finite-size EMNZ region, then the fields excited in the unbounded region outside to the finite EMNZ region are zero. Consequently, the power supplied by the classical source in the lossless limit is zero, and hence $\mathrm{Im}\, G_{uu}(\mathbf{r}',\mathbf{r}',\omega) \to 0 \quad \forall u$, and $S(\mathbf{r},\omega) = 0$. In conclusion, the spectral density of vacuum (electric field) fluctuations within bodies immersed in an ideal EMNZ host is zero.

This effect can be appreciated in Fig. 1*B*, which depicts the numerical prediction for $S(\mathbf{r},\omega)$, normalized to its free-space counterpart $S_0(\mathbf{r},\omega)$, in the presence of an EMNZ shell. For the sake of simplicity in the numerical calculations, we consider a spherical shell with internal and external radii $r_1 = 0.2\lambda$ and $r_2 = 0.3\lambda$, respectively. For comparison, Fig. 2*B* also depicts $S(\mathbf{r},\omega)$ for an epsilon-near-zero (ENZ) [i.e., $\mu(\omega) = 1, \ \varepsilon(\omega) \approx 0$] and a dielectric [i.e., $\mu(\omega) = 1, \ \varepsilon(\omega) = 4$] shells of the same geometrical characteristics. It is clear that both shells also perturb $S(\mathbf{r},\omega)$, but they do not suppress it in their whole internal regions. However, it is worth noting that the ENZ shell does suppress $S(\mathbf{r},\omega)$ at the center of the system. This effect is associated the excitation of a nonradiating mode exhibiting a spatially electrostatic distribution (with zero magnetic field) in the ENZ shell (27). Furthermore, this example reveals that, even if only nonmagnetic ($\mu = 1$) materials are available, media with near-zero parameters can still suppress vacuum fluctuations in some specific configurations.

We note that the Green function can be written as the sum of two parts, $\mathbf{G}(\mathbf{r},\mathbf{r},\omega) = \mathbf{G}_0(\mathbf{r},\mathbf{r},\omega) + \mathbf{G}_{scat}(\mathbf{r},\mathbf{r},\omega)$, corresponding to the free-space Green function [i.e., the Green function corresponding to a space empty of matter $\mathrm{Im}\, \mathbf{G}_0(\mathbf{r},\mathbf{r},\omega) = \mathbf{I} \ \omega/(6\pi c)$], and a scattering part $\mathbf{G}_{scat}(\mathbf{r},\mathbf{r},\omega)$ (i.e., the part that takes into account the scattering of the free-space fields by the background media) (21). Under this perspective, the mechanism of the EMNZ body is similar to a scattering cancellation cloak (28). That is to say, a given region of space is covered with the appropriate material to obtain a cancellation condition $\mathrm{Tr}\{\mathrm{Im}\mathbf{G}_{scat}(\mathbf{r},\mathbf{r},\omega)\} = -\mathrm{Tr}\{\mathrm{Im}\mathbf{G}_0(\mathbf{r},\mathbf{r},\omega)\}$. In this manner, the EMNZ region could also be intuitively understood as a vacuum fluctuation "cloak" at a given frequency.

Several realizations of EMNZ media have been proposed in the form of all-dielectric metamaterials (29, 30), photonic crystals (31, 32), and waveguides (33). Naturally, practical implementations of EMNZ media are necessarily dispersive (19). Therefore, just like scattering cancellation cloaks, a passive vacuum-fluctuation cloak would only be able to reduce $S(\mathbf{r},\omega)$ for a finite bandwidth (34, 35). However, as shown in the next section, this is sufficient to provide additional degrees of freedom in engineering relatively

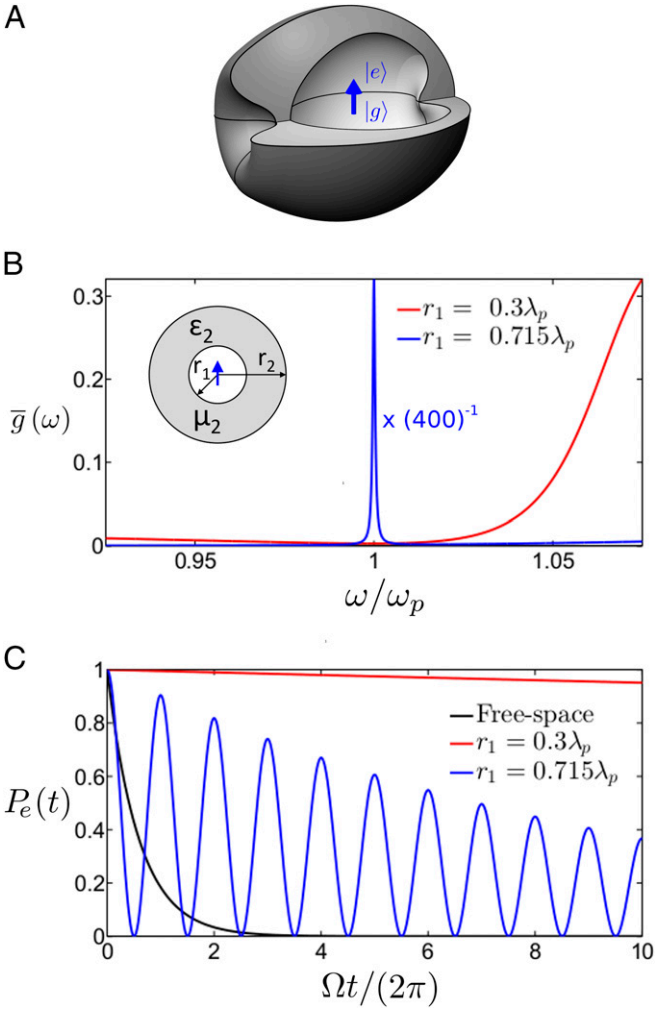

Fig. 2. Decay dynamics of a quantum emitter (QE) within an ENZ shell. (*A*) Conceptual sketch of a QE embedded within a macroscopic EMNZ shell of arbitrary shape. (*B*) Spectral density $\bar{g}(\omega)$, normalized to its free-space counterpart, for a QE positioned at the center of a spherical shell with external radius $r_2 = 1\lambda_p$, and internal radius of $r_1 = 0.3\lambda_p$ (red) and $r_1 = 0.715\lambda_p$ (blue). The shell is characterized by relative permeability, $\mu_2(\omega) = 1$, and relative permittivity, $\varepsilon_2(\omega) = 1 - \omega_p^2/(\omega(\omega + i\omega_c))$, with $\omega_p = \omega_0$, and $\omega_c = 10^{-4}\ \omega_p$. (*Inset*) Sketch of the geometry. (*C*) Time evolution of the probability of occupation of the excited state, $P_e(t)$, for nonresonant case of $r_1 = 0.3\lambda_p$ and resonant case of $r_1 = 0.715\lambda_p$ internal radii. For comparison, the black line shows the decay in free space. The magnitude of the transition dipole moment is fixed such that $\Omega = 2\pi\ 10\ \gamma$.

narrow band vacuum-fluctuation–assisted effects, for example, spontaneous emission. Furthermore, and also in analogy with advances in scattering cancellation cloaks (36), the bandwidth over which the vacuum fluctuations are reduced could be expanded by using active macroscopic media.

Decay Dynamics via Spontaneous Emission

We illustrate the applicability of EMNZ and ENZ shells as an alternative platform to engineer the decay dynamics of an initially excited QE (Fig. 2*A*). The QE is modeled as a two-level system $\{|e\rangle, |g\rangle\}$ with transition dipole moment $\mathbf{d} = \langle e|\hat{\mathbf{d}}|g\rangle$, and transition frequency ω_0. Thus, the QE and interaction Hamiltonians are given by $\hat{H}_{QE} = \hbar\omega_0\hat{\sigma}^\dagger\hat{\sigma}$ and $\hat{H}_I = \int d\omega[-\mathbf{d}\cdot\hat{\mathbf{E}}(\mathbf{r},\omega)\hat{\sigma}^\dagger + h.c.]$, respectively, with $\hat{\sigma} = |g\rangle\langle e|$. We assume that the QE is positioned at the center of a shell of internal and external radii r_1 and r_2, respectively. We show that the response of EMNZ and ENZ shells for this configuration is identical (*SI Methods*, *Spectral Density Within EMNZ and ENZ Spherical Shells*), and we simply consider an ENZ shell with relative permittivity $\varepsilon_2(\omega) = 1 - \omega_p^2/(\omega(\omega + i\omega_c))$ with $\omega_p \approx \omega_0$ (*Inset* of Fig. 2*B*).

Assuming a single excitation, the state of the system is $|\psi(t)\rangle = C_e(t)e^{-i\omega_0 t}|e\rangle|0\rangle + \int d\omega \int d^3r\ C_1(\mathbf{r},\omega,t)e^{-i\omega t}|g\rangle|1_{\mathbf{r},\omega}\rangle$, and the probability of occupation of the excited state $P_e(t) = |C_e(t)|^2$ is found refs. 6 and 37 from the solution to the following: $\partial_t C_e(t) = -\int_0^t d\tau\ K(t-\tau)C_e(\tau)$. Here, the memory kernel $K(t) = \int d\omega\ g(\omega)e^{i(\omega_0-\omega)t}$ is determined by the so-called spectral density $g(\omega) = (\omega^2/\pi\hbar\varepsilon_0 c^2)\mathbf{d}\cdot \mathrm{Im}\mathbf{G}(0,0,\omega)\cdot\mathbf{d}$, which is proportional to the density of vacuum fluctuations at the position of the QE and for the polarization of its electric dipole transition. In this canonical core–shell geometry, the spectral density at the plasma frequency is identical for EMNZ and ENZ shells, and it can be written as follows (*SI Methods*, *Spectral Density Within EMNZ and ENZ Spherical Shells*):

$$\bar{g}(\omega_p) = \frac{\omega_c}{\omega_p}\frac{k_0 r_1}{\left[\hat{J}_1(k_0 r_1)\right]^2}\frac{1}{\xi(r_1,r_2)}. \qquad [1]$$

Here, $\xi(r_1,r_2) = [1-(r_1/r_2)^3]/[1+(r_1/r_2)^3/2]$ is a geometrical parameter, and $\bar{g}(\omega_p) = g(\omega_p)/g_0(\omega_p)$, with $g_0(\omega_p) = (|\mathbf{d}|^2\ \omega_p^3)/(6\pi^2\hbar\varepsilon_0 c^3)$ being the free-space spectral density. $\hat{J}_1(x) \equiv \sqrt{\pi x/2}\ J_{3/2}(x)$, where $J_n(x)$ is the cylindrical Bessel function (38) of the first kind and order n.

Eq. **1** ratifies that $\bar{g}(\omega_p)$ vanishes as $\omega_c \to 0$, independently of the external radii r_2 and the properties of the space external to the shell. Thus, the QE decouples from the vacuum field and the dynamics of the system converge to an exponential decay $P_e(t) = \exp(-\Gamma t)$ with vanishing decay rate $\Gamma = 2\pi\ g(\omega_p) \to 0$ (note that the ENZ shell will induce a Lamb shift, which here we consider included in ω_0). In other words, the spontaneous emission is inhibited due to the influence of ENZ or EMNZ shells. At the same time, it is clear from Eq. **1** that $\bar{g}(\omega_p)$ diverges at the zeros of the Bessel function $\hat{J}_1(k_0 r_1) = 0$, corresponding to the excitation of bound eigenmodes with spatially electrostatic field distributions studied in refs. 27, 39, and 40. In fact, we find that the spectral density for this resonant internal radius asymptotically converges to a Lorentzian line given by the following (*SI Methods*, *Spectral Density Within EMNZ and ENZ Spherical Shells*):

$$\bar{g}(\omega) = \frac{f_g}{\pi}\frac{\gamma^2}{(\omega-\omega_p)^2+\gamma^2}, \qquad [2]$$

with oscillator strength,

$$f_g = f_{g\infty}\ \xi(r_1,r_2), \qquad [3]$$

and linewidth,

$$\gamma = \gamma_\infty\frac{\hat{J}'_1(k_0 r_1) - \frac{1}{2}}{\hat{J}'_1(k_0 r_1) - \frac{1}{2}\xi(r_1,r_2)}, \qquad [4]$$

where $\hat{J}_1{}'(x) \equiv \partial_x\hat{J}_1{}'(x)$. In addition, $f_{g\infty} = \lim_{r_2\to\infty} f_g$ and $\gamma_\infty = \lim_{r_2\to\infty}\gamma$ are the asymptotic values of the oscillator strength and linewidth in the large shell limit, $r_2 \to \infty$. Explicit expressions of $f_{g\infty}$ and γ_∞ are reported in *SI Methods*, *Spectral Density Within EMNZ and ENZ Spherical Shells*, although they can be roughly approximated by $\gamma_\infty \sim \omega_c/3$ and $f_{g\infty} \sim \pi c/\omega_c r_1$. The validity of this asymptotic limit is checked in Fig. S1. Note that the interaction of a QE with a Lorentzian line has a well-known solution (6), which results in the excitation of non-Markovian reversible processes in the form of Rabi oscillations, $P_e(t) = \exp(-\Gamma t)\cos^2(\Omega t/2)$, with frequency $\Omega = 2\sqrt{g_0(\omega_p) f_g}\gamma$.

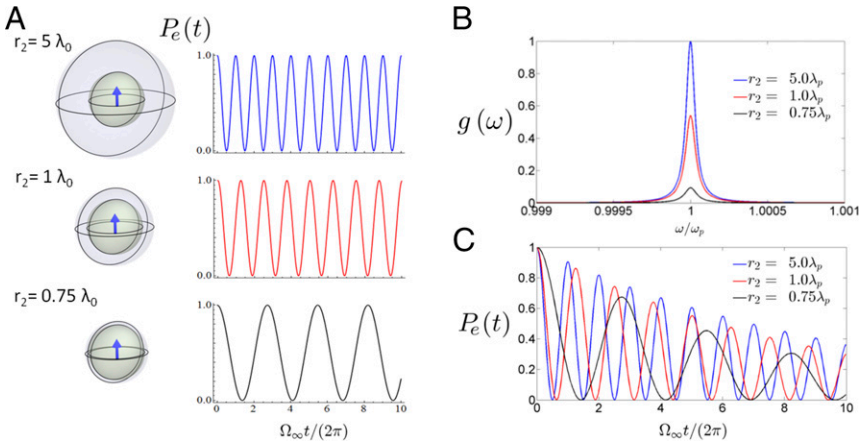

Fig. 3. Decay dynamics under deformations of the external boundary. (*A*) Sketch of the geometry (not drawn to scale) and time evolution of the probability of occupation of the excited state, $P_e(t)$, for an ideally lossless ENZ shell [$\varepsilon_2(\omega) = 1 - \omega_p^2/(\omega(\omega + i\omega_c))$, $\omega_p = \omega_0$, and $\omega_c = 0$] with resonant internal radius $r_1 = 0.715\lambda_p$, and for different external different radii r_2. (*B*) Spectral density, $g(\omega)$, normalized to the maximal computed value, for a lossy ENZ shell ($\omega_c = 10^{-4}\ \omega_p$) for different external radii. (*C*) Time evolution of the probability of occupation of the excited state, $P_e(t)$, for the lossy ENZ shell. The magnitude of the transition dipole moment is fixed so that $\Omega_\infty = 2\pi\ 10\ \gamma_\infty$.

Therefore, we conclude that, on the one hand, EMNZ and ENZ shells enable the suppression of spectral density and consequent inhibition of spontaneous emission, whereas, on the other hand, they also enable the controlled excitation of bound eigenmodes, and thus the potential triggering of reversible decay dynamics. Both effects can be clearly appreciated in Fig. 2 *B* and *C*, which represent, respectively, the normalized spectral density and the time evolution of the probability of occupation of the excited state, $P_e(t)$, for a shell with external radius $r_2 = \lambda_p$, and for examples of nonresonant $r_1 = 0.3\lambda_p$ and resonant $r_1 = 0.715\lambda_p$ internal radii. For illustrative purposes, we set $\omega_c = 10^{-4}\omega_p$ so that the resonance exhibits a linewidth on the same order of magnitude than those observed in the synthetic implementations presented later in Fig. 4. We also select the transition dipole moment such that $\Omega = 2\pi\ 10\ \gamma$, that is, so that we can clearly view and appreciate reversible dynamics with 10 oscillations before the probability of occupation decays to $\exp(-1) \sim 0.37$. The figures confirm that $g(\omega_p)$ and the spontaneous emission are suppressed for the nonresonant radius, $r_1 = 0.3\lambda_p$, whereas a resonant line and Rabi oscillations are observed for the resonant radius $r_1 = 0.715\lambda_p$.

In a way, the inhibition of spontaneous emission and subsequent excitation of bound eigenmodes in EMNZ and ENZ shells could be considered somewhat analogous to the response of photonic band gap and defect cavity modes in PCs, and/or single-mode closed cavities. However, by contrast with PCs and closed cavities, the EMNZ and ENZ shells can be of any size and shape (39), and it is also accessible from the outside by using nonlinear media (41). On top of that, we now demonstrate that it also provides additional degrees of freedom in tuning and engineering the decay dynamics that are essentially different from those of conventional cavities and PCs. To this end, we note that one remarkable property of the eigenmodes excited in EMNZ and ENZ shells is that their eigenfrequency is invariant with respect to geometrical transformations of the external boundary of the shell (39). This is in fact reflected in Eq. **2**, because the resonant frequency of the Lorentzian line equals ω_p independently of r_2. Next, we note from Eqs. **2**–**4** that compressing the shell from an infinite size ($r_2 \to \infty$) to an infinitesimal thickness ($r_2 \to r_1$), shifts the vacuum Rabi frequency from $\Omega_\infty = \lim_{r_2 \to \infty} \Omega \approx 2\sqrt{(\pi c/3r_1)g_0(\omega_p)}$ to $\Omega_0 = \lim_{r_2 \to 0} \Omega = 0$.

This effect is quite different from the behavior of conventional cavities. In fact, the resonance frequency of a conventional cavity is shifted by changing its size. Here, by contrast, we find that it is the vacuum Rabi frequency associated to a bound eigenmode (with fixed eigenfrequency) that changes as a function of the shell size (not the resonance frequency of the cavity). This effect is illustrated in Fig. 3*A*, which depicts time evolution of the probability of occupation of the excited state $P_e(t)$ for ideally lossless ENZ shells with resonant internal radius $r_1 = 0.715\lambda_p$ and for different external radii. Therefore, in the same wave that perturbing a conventional cavity allow us to finely tune the resonance frequency (as it is done, for example, by introducing a screw in microwave cavities), we find that deforming a zero-index cavity enables us to finely tune the vacuum Rabi frequency without detuning the eigenfrequency of the cavity. Naturally, in the presence of losses, there is a nonzero resonance linewidth that would increase from $\gamma_\infty \sim \omega_c/3$ to $\gamma_\infty \sim \omega_c/2$ when compressing the cavity. This effect can be appreciated in Fig. 3*B*, which depicts the spectral density $g(\omega)$ normalized to its peak value in the large shell limit $g_\infty(\omega_p) = \lim_{r_2 \to \infty} g(\omega_p)$, for losses $\omega_c = 10^{-4}\ \omega_p$. Consequently, the oscillations in $P_e(t)$ will be exponentially damped as it can be appreciated in Fig. 3*C*.

This is an example of the qualitatively different physics that could be observed using ZI shells as an alternative platform for manipulating light–matter interactions. Moreover, we emphasize that the same effect would appear in ENZ shells with an arbitrarily shaped external boundary (see Fig. S2 for the analysis of a cubic cavity with "screw-like" deformations). It is also worth remarking that this effect is essentially different from detuning in conventional cavities, which decreases the strength of the oscillations as shown in Fig. S3. We anticipate that many other unique phenomena might emerge in more advanced configurations including complex QEs (e.g., multilevel or higher-order transitions), multimode cavities, more complex photonic states, systems driven by an external source, opto- and acousto-mechanical systems, etc.

Synthetic Implementations

The losses of naturally available ENZ materials might be too high to observe the effects predicted in Figs. 2 and 3. On the bright side, research on exotic phenomena excited in complex media is often transferred into the development of synthetic implementations of those effects that otherwise might have not been possible. Following this line of thought, we now demonstrate that decay dynamics identical to those induced by an ENZ shell can be excited in suitably designed cylindrical core–shell microwave resonators. We expect that this will facilitate the experimental validation of our theoretical results. The geometry of the proposed resonator is schematically depicted in Fig. 4*A*. It consists of a core–shell cylindrical resonator of internal and external radii r_1 and r_2, respectively. Furthermore, the substance filling the core and shell regions are assumed to be characterized by relative permittivity $\varepsilon_1 = 10$ and $\varepsilon_2 = 1$, respectively. We assume that this closed resonator is bounded by copper walls with finite conductivity (24) $\sigma = 5.7\ 10^7$ S/m, although much higher

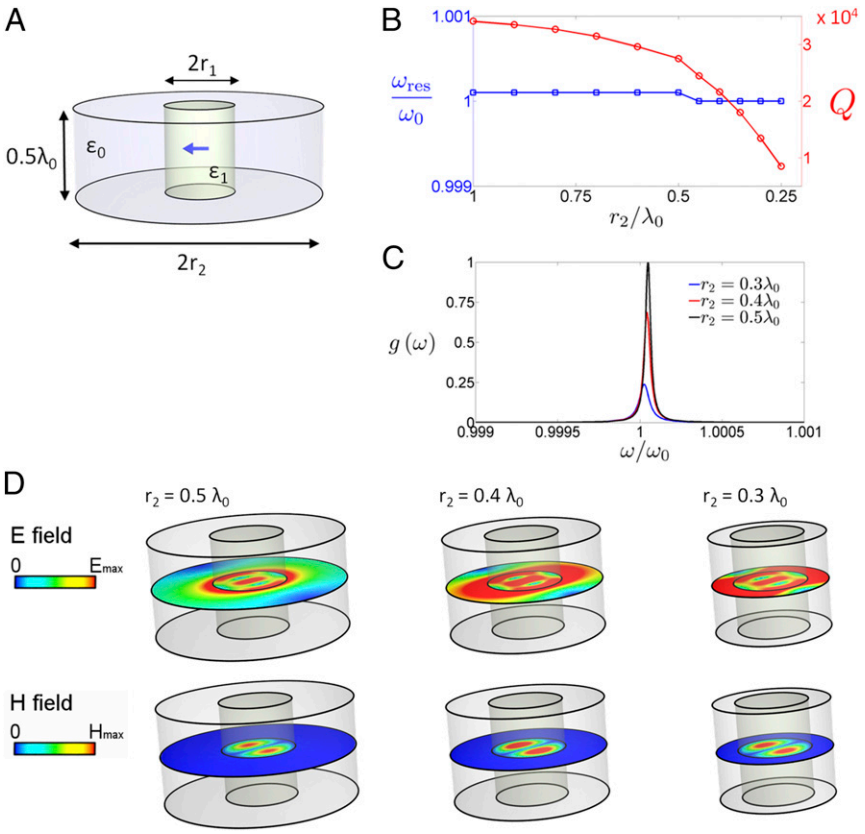

Fig. 4. Synthetic implementation of ENZ shells as a microwave cylindrical resonator. (*A*) Geometry of the resonator: cylindrical resonator of height $h=0.5\lambda_0$ (with arbitrarily chosen value $\lambda_0=0.03$ m at 10 GHz) and radius r_2, containing a dielectric rod of relative permittivity $\varepsilon_1=10$ and whose radius is set to satisfy the resonance condition $J_1(\beta_1 r_1)=0$ ($r_1\sim 0.2\lambda_0$). The resonator is bounded by copper walls ($\sigma=5.7\ 10^7$ S/m). Numerically simulated performance: (*B*) Eigenfrequency, ω_{res}, and quality factor Q, as a function of the external radius r_2. (*C*) Spectral density, $g(\omega)$, normalized to the maximal computed value, for a QE located at $\boldsymbol{r}=(0,0,h/2)$ with its dipole moment pointing along $\hat{x}$ for three different external radii. (*D*) Electric and magnetic field magnitude distributions excited by such QE in the middle plane ($z=h/2$).

quality factors could be easily obtained with superconducting cavities (42, 43).

Following other synthetic implementations of zero-index media in parallel-plate waveguides (33, 44), the height of the resonator is set to $h=0.5\lambda_0$. However, here we study the $\text{TE}^{11\text{e}}$ and $\text{TM}^{11\text{o}}$ modes (38), whose explicit expressions for the field distribution are reported in *SI Methods*, *Cylindrical Core–Shell Resonator*. Although the field expressions are involved, the response of the system is simple: in the $h\to 0.5\lambda_0$ limit, the transversal propagation constant, $\beta^2=(\omega^2/c^2)-(\pi/h)^2$, vanishes in the air-filled region. Then, the $\text{TE}^{11\text{e}}$ and $\text{TM}^{11\text{o}}$ modes collapse in the ($\varepsilon_2=1$) shell region into a single mode, whose field distribution in the middle plane ($z=h/2$) is identical to that excited by a 2D electrostatic dipole. In turn, the degeneracy in the shell provides the necessary degrees of freedom to ensure that, if we set the internal radius such that $J_1(\beta_1 r_1)=0$, then the resonator supports a hybrid $\text{TE}^{11\text{e}}$–$\text{TM}^{11\text{o}}$ eigenmode independently of the external radius r_2. This effect is clearly analogous to the localized mode excited in the spherical ENZ shell, which appears for $\hat{J}_1(k_0 r_1)=0$ (Eq. **1**), independently of its external radius r_2, and also exhibiting a spatially electrostatic field distribution.

To numerically test this effect, the core radius is set to satisfy $J_1(\beta_1 r_1)=0$ ($r_1\sim 0.2\lambda_0$), and the external radius is compressed from $1\lambda_0$ to $0.25\ \lambda_0$. The computed eigenfrequencies and quality factors, depicted in Fig. 4*B*, reveal that the resonance frequency only shifts a 0.01% when compressing the external boundary. On the contrary, the quality factor Q changes from 34,105 to 8,517. Then, if a QE is placed at the center of the resonator, it would mostly couple to this resonant mode, leading to dynamics as a function of the external radius similar to those depicted in Fig. 3. This effect is confirmed by computing $g(\omega)$ for three different external radii $r_2=0.3\lambda_0$, $0.4\lambda_0$, and $0.5\lambda_0$ (Fig. 4*C*). As expected, $g(\omega)$ is characterized by a clear resonant line. In analogy with Fig. 3*B*, it is found that compressing the cavity from $r_2=0.5\lambda_0$ to $r_2=0.3\lambda_0$ reduces the peak of $g(\omega)$ to a 24% of its original value without a significant detuning. In fact, the residual detuning, smaller than the linewidth, might be attributed to numerical precision. To complete the description, the electric and magnetic field magnitude distributions in the middle plane ($z=h/2$) and at the peaks of $g(\omega)$ are reported in Fig. 4*D*. It is clear from the figure that field distribution in the shell region does indeed feature a spatially electrostatic (but temporally dynamic) field distribution in the middle plane.

We emphasize that, although we have studied the response of a closed core–shell cylindrical cavity, the same design strategy could be applied to a variety of configurations. In fact, the proposed resonator is very robust against deformations of the external boundary, and hence cylindrical resonators with arbitrary cross-sections could be used in practice (Fig. S4). Moreover, open systems with similar characteristics can be designed by using patterned surfaces that enforce the appropriate boundary conditions (45) (Fig. S5).

Therefore, our results suggest that the proposed theoretical concepts could be experimentally validated in a number of microwave resonators. For instance, these resonators could be integrated into traditional setups for experiments of Rydberg atoms interacting with microwave photons in superconducting cavities (18). Also at microwave frequencies, most recent advances in research of vacuum fluctuations have been carried out in waveguide-based superconducting circuits (3). Thus, a promising line of research might be to redesign waveguide structures exhibiting zero-index modes [e.g., rectangular metallic waveguides at cutoff (33, 44), and/or transmission lines loaded with lumped elements (46)], to be integrated into those systems and observe the predicted effects. As for scaling the system to higher frequency regimes, there is a variety continuous media that exhibit ENZ properties at infrared frequencies. The moderate losses of these materials [e.g., $\varepsilon\approx i0.03$ for silicon carbide at

$\lambda \sim 10.33$ μm (47, 48), and $\varepsilon \approx i0.1 \sim i0.2$ for aluminum-doped zinc oxide at telecom wavelengths (49, 50)] might enable the observation of vacuum fluctuations being weakened, but they are most probably to too high to observe strong coupling with bound eigenmodes. A low-loss alternative at optical frequencies could be all-dielectric, and thus low-loss, specially designed photonics crystals (31, 32) and/or metamaterials (29, 30), exhibiting propagation and scattering features similar to those of zero-index media. However, the nonnegligible size of the dielectric particles constituting these structures result in spatial dispersion, and additional design efforts would be required to circumvent this effect and couple the emitter to the desired mode.

Conclusions

Our theoretical study demonstrates that ZI structures enable the inhibition and manipulation of vacuum fluctuations and their associated effects. We believe that this result presents an important step forward in our understanding of the interaction of macroscopic bodies with quantum fields, and ZI structures are suggested as an alternative platform to investigate light–matter interactions. We expect that unique phenomena might emerge from distinctive features of ZI structures, such as the possibility of dynamically deforming the platform without introducing a shift in the eigenfrequencies of bound eigenmodes. The possibility of designing different synthetic implementations that emulate the response of ZI media facilitates the future experimental validation and further exploration of these concepts.

Methods

All numerical simulations were carried out with the commercially available full-wave electromagnetic simulator software COMSOL Multiphysics, version 5.0 (https://www.comsol.com/). The spectral density of vacuum (electric field) fluctuations $S(\boldsymbol{r}, \omega)$ and the spectral density $g(\omega)$ in Figs. 1*B* and 4*C*, and Fig. S2 were computed by evaluating the Green dyadic function with the frequency domain solver. The eigenfrequency values, quality factors, and eigenmodes depicted in Fig. 4*B* and Fig. S4 were computed with the eigenfrequency solver. The solver was requested to search for eigenfrequencies around ω_0, and it reported complex eigenfrequency values $\omega' = \omega_{\text{res}} + i\alpha$, with an associated field distribution. Subsequently, ω_{res} was identified as the eigenfrequency value, and the quality factor was computed as $Q = \omega_{\text{res}}/(2|\alpha|)$. The spectral density $g(\omega)$ depicted in Figs. 2*B* and 3*B*, and Fig. S1 was computed from the analytical solution to the problem provided in *SI Methods*, *Spectral Density Within EMNZ and ENZ Spherical Shells*. The time evolution of the probability of occupation of the excited state $P_e(t)$ in Figs. 2*C* and 3*C*, and Fig. S3 was computed by fitting the spectral density to a series of Lorentzians and applying the inverse Laplace transform to the memory kernel.

ACKNOWLEDGMENTS. The authors would like to acknowledge partial support from the Vannevar Bush Faculty Fellowship program sponsored by the Basic Research Office of the Assistant Secretary of Defense for Research and Engineering and funded by the Office of Naval Research through Grant N00014-16-1-2029, and partial support from US Air Force Office of Scientific Research Multidisciplinary University Research Initiative (MURI) on Quantum Metaphotonics and Metamaterials Award FA9550-12-1-0488.

1. Scully MO, Zubairy MS (1997) *Quantum Optics* (Cambridge Univ Press, Cambridge, UK).
2. Milonni PW (1994) *The Quantum Vacuum: An Introduction to Quantum Electrodynamics* (Academic, New York).
3. Nation PD, Johansson JR, Blencowe MP, Nori F (2012) Stimulating uncertainty: Amplifying the quantum vacuum with superconducting circuits. *Rev Mod Phys* 84(1):1–24.
4. Jaffe RL (2005) Casimir effect and the quantum vacuum. *Phys Rev D Part Fields Gravit Cosmol* 72(2):21301.
5. Riek C, et al. (2015) Direct sampling of electric-field vacuum fluctuations. *Science* 350(6259):420–423.
6. Vogel W, Welsch D-G (2006) *Quantum Optics* (Wiley, Berlin).
7. Lamb WE, Retherford RC (1947) Fine structure of the hydrogen atom by a microwave method. *Phys Rev* 72(3):241–243.
8. Dalvit D, Milonni P, Roberts D, da Rosa F (2011) *Casimir Physics* (Springer, Berlin).
9. Novotny L, Hecht B (2006) *Principles of Nano-Optics* (Cambridge Univ Press, Cambridge, UK).
10. Silveirinha MG (2014) Theory of quantum friction. *New J Phys* 16(6):63011.
11. Purcell EM (1946) Spontaneous emission probabilities at radio frequencies. *Phys Rev* 69:681.
12. Bykov VP (1975) Spontaneous emission from a medium with a band spectrum. *Sov J Quantum Electron* 4(7):861–871.
13. Yablonovitch E (1987) Inhibited spontaneous emission in solid-state physics and electronics. *Phys Rev Lett* 58(20):2059–2062.
14. John S, Wang J (1990) Quantum electrodynamics near a photonic band gap: Photon bound states and dressed atoms. *Phys Rev Lett* 64(20):2418–2421.
15. John S, Quang T (1994) Spontaneous emission near the edge of a photonic band gap. *Phys Rev A* 50(2):1764–1769.
16. Kleppner D (1981) Inhibited spontaneous emission. *Phys Rev Lett* 47(4):233–236.
17. Hulet RG, Hilfer ES, Kleppner D (1985) Inhibited spontaneous emission by a Rydberg atom. *Phys Rev Lett* 55(20):2137–2140.
18. Haroche S, Raimond JM (2006) *Exploring the Quantum* (Oxford Univ Press, Oxford).
19. Engheta N, Ziolkowski RW (2006) *Metamaterials: Physics and Engineering Explorations* (Wiley, Hoboken, NJ).
20. Ziolkowski RW (2004) Propagation in and scattering from a matched metamaterial having a zero index of refraction. *Phys Rev E Stat Nonlin Soft Matter Phys* 70(4 Pt 2):046608.
21. Scheel S, Knoll L, Welsch D-G (1999) Spontaneous decay of an excited atom in an absorbing dielectric. *Phys Rev A* 60(5):4094–4104.
22. Tai CT, Collin RE (2000) Radiation of a hertzian dipole immersed in a dissipative medium. *IEEE Trans Antenn Propag* 48(10):1501–1506.
23. Scheel S, Buhmann SY (2008) Macroscopic quantum electrodynamics—concepts and applications. *Acta Phys Slovaca* 58(5):675–809.
24. Balanis CA (2012) *Advanced Engineering Electromagnetics* (Wiley, Hoboken, NJ), 2nd Ed.
25. Lindell IV, Sihvola AH (2009) Electromagnetic boundary and its realization with anisotropic metamaterial. *Phys Rev E Stat Nonlin Soft Matter Phys* 79(2 Pt 2):026604.
26. Rumsey V (1959) Some new forms of Huygens' principle. *IRE Trans Antennas Propag* 7(5):103–116.
27. Liberal I, Engheta N (2016) Nonradiating and radiating modes excited by quantum emitters in open epsilon-near-zero cavities. *Sci Adv* 2(10):e1600987.
28. Alù A, Engheta N (2005) Achieving transparency with plasmonic and metamaterial coatings. *Phys Rev E Stat Nonlin Soft Matter Phys* 72(1 Pt 2):016623–016631.
29. Moitra P, et al. (2013) Realization of an all-dielectric zero-index optical metamaterial. *Nat Photonics* 7:791–795.
30. Maas R, Parsons J, Engheta N, Polman A (2013) Experimental realization of an epsilon-near-zero metamaterial at visible wavelengths. *Nat Photonics* 7(October):907–912.
31. Huang X, Lai Y, Hang ZH, Zheng H, Chan CT (2011) Dirac cones induced by accidental degeneracy in photonic crystals and zero-refractive-index materials. *Nat Mater* 10(8):582–586.
32. Li Y, et al. (2015) On-chip zero-index metamaterials. *Nat Photonics* 9(11):738–742.
33. Mahmoud AM, Engheta N (2014) Wave-matter interactions in epsilon-and-mu-near-zero structures. *Nat Commun* 5:5638.
34. Monticone F, Alù A (2014) Do cloaked objects really scatter less? *Phys Rev X* 3(4):1–10.
35. Sohl C, Gustafsson M, Kristensson G (2007) Physical limitations on broadband scattering by heterogeneous obstacles. *J Phys A* 40(36):11165–11182.
36. Miller DAB (2006) On perfect cloaking. *Opt Express* 14(25):12457–12466.
37. González-Tudela A, Huidobro PA, Martín-Moreno L, Tejedor C, García-Vidal FJ (2014) Reversible dynamics of single quantum emitters near metal-dielectric interfaces. *Phys Rev B* 89(4):41402.
38. Harrington RF (1961) *Time-Harmonic Electromagnetic Fields* (McGraw-Hill, New York).
39. Liberal I, Mahmoud AM, Engheta N (2016) Geometry-invariant resonant cavities. *Nat Commun* 7:10989.
40. Silveirinha MG (2014) Trapping light in open plasmonic nanostructures. *Phys Rev A* 89(2):23813.
41. Lannebère S, Silveirinha MG (2015) Optical meta-atom for localization of light with quantized energy. *Nat Commun* 6:8766.
42. Kuhr S, et al. (2007) Ultrahigh finesse Fabry-Pérot superconducting resonator. *Appl Phys Lett* 90(16):164101.
43. Meschede D, Walther H, Müller G (1985) One-atom maser. *Phys Rev Lett* 54(6):551–554.
44. Rotman W (1962) Plasma simulation by artificial dielectrics and parallel-plate media. *Antennas Propagation. IRE Trans* 10(1):17–19.
45. Della Giovampaola C, Engheta N (2016) Plasmonics without negative dielectrics. *Phys Rev B* 93:195152.
46. Eleftheriades GV, Balmain KG (2005) *Negative-Refraction Metamaterials: Fundamental Principles and Applications* (Wiley, Hoboken, NJ).
47. Caldwell JD, et al. (2015) Low-loss, infrared and terahertz nanophotonics using surface phonon polaritons. *Nanophotonics* 4(1):44–68.
48. Kim J, et al. (2016) Role of epsilon-near-zero substrates in the optical response of plasmonic antennas. *Optica* 3(3):339–346.
49. Kinsey N, Ferrera M, Shalaev VM, Boltasseva A (2015) Examining nanophotonics for integrated hybrid systems: A review of plasmonic interconnects and modulators using traditional and alternative materials. *J Opt Soc Am B* 32(1):121–142.
50. Kinsey N, et al. (2015) Epsilon-near-zero Al-doped ZnO for ultrafast switching at telecom wavelengths. *Optica* 2(7):616–622.